Journal of Crystal Growth 450 (2016) 174–180

Contents lists available at ScienceDirect

Journal of Crystal Growth

journal homepage: www.elsevier.com/locate/jcrysgro

Rice-like hollow nano-$CaCO_3$ synthesis

Eda Ulkeryildiz, Sevgi Kilic, Ekrem Ozdemir *

Department of Chemical Engineering, Izmir Institute of Technology, Gulbahce Campus, Urla, Izmir, Turkey

ARTICLE INFO

Article history:
Received 21 April 2016
Received in revised form
16 June 2016
Accepted 17 June 2016
Available online 24 June 2016

Keywords:
Hollow
Nano
$CaCO_3$
$Ca(OH)_2$
Stability
Zeta potential

ABSTRACT

We have shown that $Ca(OH)_2$ solution is a natural stabilizer for $CaCO_3$ particles. We designed a CO_2 bubbling crystallization reactor to produce nano-$CaCO_3$ particles in homogenous size distribution without aggregation. In the experimental set-up, the crystallization region was separated from the stabilization region. The produced nanoparticles were removed from the crystallization region into the stabilization region before aggregation or crystal growth. It was shown that rice-like hollow nano-$CaCO_3$ particles in about 250 nm in size were produced with almost monodispersed size distribution. The particles started to dissolve through their edges as CO_2 bubbles were injected, which opened-up the pores inside the particles. At the late stages of crystallization, the open pores were closed as a result of dissolution-recrystallization of the newly synthesized $CaCO_3$ particles. These particles were stable in $Ca(OH)_2$ solution and no aggregation was detected. The present methodology can be used in drug encapsulation into inorganic $CaCO_3$ particles for cancer treatment with some modifications.

1. Introduction

Calcium carbonate ($CaCO_3$) is one of the most abundant minerals in nature and widely used as filling material in various industries in order to decrease the product costs and to improve some of the mechanical properties of the composite materials. The enhancement in the physical and mechanical properties of the polymeric composite materials is more pronounced when the particles are in nano sizes [1]. It could be possible to produce $CaCO_3$ from its natural mineral sources by crushing, grinding, and sieving processes. However, calcite produced from natural sources are in micron sizes and they have inhomogeneous size distribution [2]. Therefore, production of nano calcite can be achieved by recrystallization; such that the mineral $CaCO_3$ is converted to calcium oxide (CaO) by calcination, hydrated to calcium hydroxide ($Ca(OH)_2$) and recrystallize by carbon dioxide (CO_2) [3–6]. Obtaining $CaCO_3$ particles in nano sizes with homogeneous size distribution and different morphologies is difficult due to agglomeration of newly synthesized clusters [7–10], which is related to the surface potential of the colloidal $CaCO_3$ particles [11–14]. Also, there is a huge effort to produce hollow nano-$CaCO_3$ particles with homogenous size distribution and different morphologies, which is rare in the literature.

Classical crystallization mechanisms claim that a nucleation step is required before crystal growth [15]. However, novel crystallization mechanisms require a prenucleation process in which ions form stable clusters [7]. These clusters are charged particles in equilibrium with their ions and they can grow or collide to produce $CaCO_3$ nuclei. Therefore, certain additives were introduced into the crystal growing medium to alter the surface charge of the growing nuclei and to inhibit the $CaCO_3$ growth [16–19]. Nano-$CaCO_3$ particles can be produced when the newly produced particles are stabilized by adjusting the surface potential of the particles. The surface potential of the colloidal system is related to the magnitude of the zeta potential. Particles with zeta potentials more positive than +30 mV or more negative than −30 mV are considered stable [20]. The zeta potential values for the $CaCO_3$ have been reported in the literature sometimes positive, sometimes negative, and sometimes variable zeta potential values [13]. The point of zero charge (PZC) of $CaCO_3$ exists around 9–10 although the zeta potential of colloids is pH-dependent [21]. The zeta potential for $CaCO_3$ was reported to be about −10 mV [22] indicating that the newly produced $CaCO_3$ clusters are naturally unstable. It is the reason why newly formed particles were aggregated and formed micron sized particles [3,9,23–27]. It was understood that the surface potential for $CaCO_3$ is affected by various parameters such as aging [22], additives [28], surface modifiers [11], and ions [12,14]. For instance, the zeta potential for $CaCO_3$ was positive when Ca^{++} ions were in excess in the solution, and it was negative when CO_3^{2-} ions were in excess in the solution [12,14,22]. Therefore, the presence of other ions, called the potential determining ions (PDI) [13] such as crystal lattice ions, surface hydrolysis ions, and adsorbing ions in solution, are

* Corresponding author.
E-mail address: ekremozdemir@iyte.edu.tr (E. Ozdemir).

http://dx.doi.org/10.1016/j.jcrysgro.2016.06.032
0022-0248/

highly important for the production of stable nano-$CaCO_3$ particles.

In our previous paper [29], we have reported that the zeta potential for $CaCO_3$ particles was more than +30 mV in $Ca(OH)_2$ solution and the $Ca(OH)_2$ solution is indeed a natural stabilizer for the newly produced $CaCO_3$ particles. We now propose that nano-$CaCO_3$ particles could be produced in homogenous size distribution when the stability of the clusters could be achieved in the colloidal solution. Here, an experimental strategy was developed, for which the newly produced nano clusters were removed from the crystallization region into the stabilization region and show that, for the first time, the nano-particles of about 300 nm in size, homogenous size distribution, and rice-like hollow calcite particles can be produced.

2. Materials and methods

2.1. Materials

Calcium hydroxide ($Ca(OH)_2$) was purchased from Merck with a purity of 96% of which 3% was $CaCO_3$, and 1% was other impurities (mainly 0.05% of Na, K, Fe, Sr; 0.5% of Mg; 0.01% of SO_4^{2-}, and 0.005% of Cl^-). CO_2 gas was purchased from Carbogas, Turkey with a purity of 99.99%. Ultrapure water was obtained with a MilliQ (Millipore-Elix UV5/ Milli-Q) water purification system with a resistivity of 18.2 MΩ cm at 25 °C.

2.2. Experimental set-up

The $CaCO_3$ crystallization was performed in a stirred tank reactor at room temperature as shown in Fig. 1. The reactor consists of a crystallization tank filled with ultra-pure water, a mechanical stirrer, a CO_2 bubbling orifice, a pH meter with conductivity probe, and a data acquistion system. The CO_2 gas was bubbled from the CO_2 tank through an orifice into the $Ca(OH)_2$ solution. The vicinity of CO_2 bubbles was termed as "crystallization region". The remaining undissolved CO_2 bubbles was allowed to be purged from the surface of the solution to the atmosphere. The newly formed $CaCO_3$ crystal particles around the CO_2 bubbles were removed as quickly as possible from the crystallization region into the $Ca(OH)_2$ solution by mechanical stirring. The CO_2 bubble-free region of the reactor is called the "stabilization region". 15 mM of $Ca(OH)_2$ solution was prepared by adding 7.78 g of $Ca(OH)_2$ powders in 7 L of ultra-pure water and allowed to dissolve by stirring at 750 RPM for 30 min before the CO_2 injection. Conductivity and pH values were measured and monitored by Thermo Orion 5-star pH meter and recorded with a Thermo Star Navigator 21 software program.

2.3. Sample preparation and characterization

Average particle size, size distribution, and zeta potential values were measured using dynamic light scattering (DLS) method. About 1 ml of sample was withdrawn from the solution into a UV cuvette and size and size distribution were measured using particle size analyzer (Malvern nano sizer, ZS model). A 1 ml of sample was also withdrawn from the solution into a zeta cell and zeta potential values were measured.

At certain time interval, precipitates were separated from sampled solutions by centrifugation (Universal 320 – Hettich Zentrifugen) at 9000 RPM for 20 min. The particles were washed with acetone and dried at 103 °C in an oven (Nüve FN 500) overnight. The morphologies of the $CaCO_3$ crystals were analyzed using a scanning electron microscope (SEM) equipped with a field emission source (Philips XL 30S FEG), operating at an accelerating voltage of 15 kV. The crystal structure of the particles was determined by the X-ray powder diffraction (XRD) measurements.

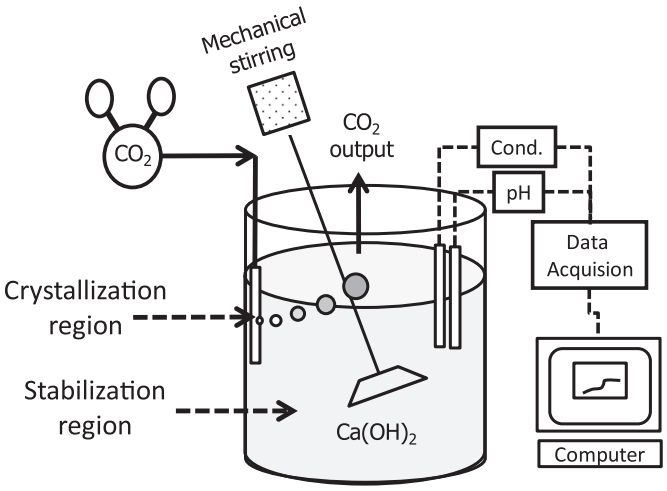

Fig. 1. Experimental set-up.

3. Results and discussion

Because calcium carbonate crystallization is an ionic reaction, the crystal growth rate cannot be easily controlled, and thus, it is difficult to obtain particles in nano sizes, homogeneous size distribution, and different morphologies. In order to understand the phenomena occurring in $CaCO_3$ crystallization in $Ca(OH)_2$ as in the carbonization method, the zeta potential values of $CaCO_3$ particles in $Ca(OH)_2$ solution were investigated and reported recently in our previous paper [29]. The dissolution of $CaCO_3$ and $Ca(OH)_2$ powders both produced ions such as Ca^{++}, , OH^-, and $Ca(OH)^+$ as well as newly synthesized nano-$CaCO_3$ particles in the solution. The zeta potential values were measured to be always positive in $Ca(OH)_2$ solution due to an imbalance between Ca^{++} and CO_3^{2-} ions, so called the potential determining ions (PDI), present in the solution. It was concluded that the zeta potential of $CaCO_3$ particles is more than +30 mV and therefore they must be stable in the $Ca(OH)_2$ solution so that nano-$CaCO_3$ particles could be synthesized without aggregation. The present experimental method was designed to stabilize the newly generated nano-$CaCO_3$ particles in $Ca(OH)_2$ solution.

Fig. 2 shows the change in conductivity and pH values during the progress in the $CaCO_3$ crystallization in the CO_2 bubbling

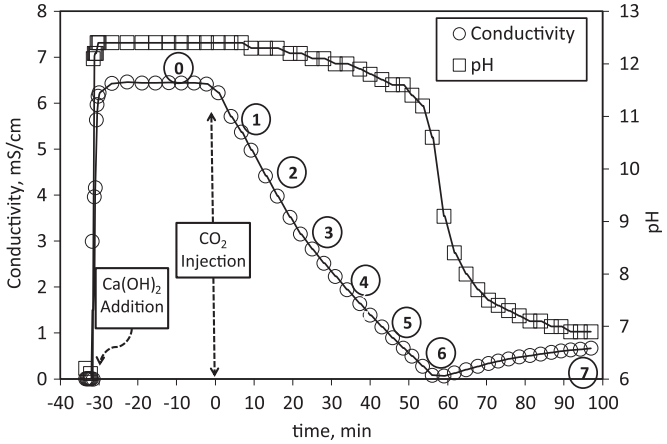

Fig. 2. Change in conductivity and pH during the progress in the $CaCO_3$ crystallization in a CO_2 bubbling stirred reactor.

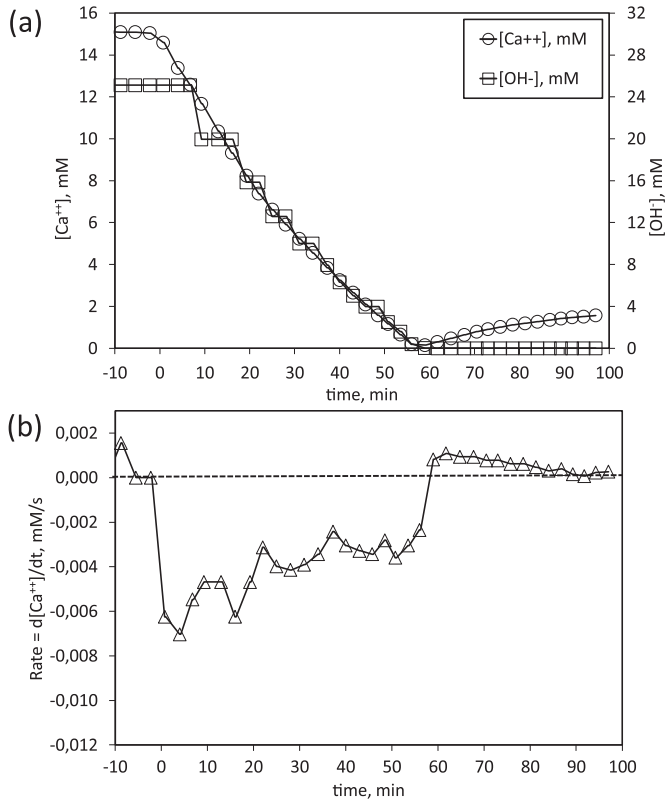

Fig. 3. (a) Calculated [Ca^{++}] and [OH^-] ion concentrations in solution and (b) Ca^{++} ion consumption rate during $CaCO_3$ crystallization.

stirred reactor. As shown in figure, before the CO_2 injection, the conductivity and pH values for pure water were constant at 0.90 μs/cm and 5.5, respectively. When $Ca(OH)_2$ were added into the pure water, pH was reached to 12.5 and conductivity was reached to 6.6 mS/cm and the solution was fully stabilized in about 10 minutes. As soon as the CO_2 was injected into the system in bubble form, almost a linear decrease in the conductivity and a slight decrease in pH were observed at the early stage of crystallization. The decrease in conductivity was related to the consumption of Ca^{++} ions in the solution [29]. As can be seen from the conductivity values, the crystallization rate seems to be higher at the earlier stages of crystallization and it was relatively slower during the late stages of the crystallization. Decrease of the conductivity to about 0 mS/cm value indicated that almost all of Ca^{++} ions were consumed in the solution. At this stage, a steep decrease in pH was observed due to increase in H^+ and HCO_3^- ion concentrations in the solution as a result of CO_2 dissolution. The pH values were greater than 11.5 during the early stages of the $CaCO_3$ crystallization, which is important on the formation of calcite form among $CaCO_3$ polymorphs [26]. The decrease in pH resulted in the dissolution of some of the already precipitated or crystallized $CaCO_3$ particles in the solution, which yielded the conductivity to increase back again in the solution. The crystallization was terminated when pH reached to about 7.0. Samples were taken at the specified time intervals as shown in the figure.

The [Ca^{++}] and [OH^-] ion concentrations can be estimated from the conductivity and pH values, respectively. We have shown that the measured conductivity values is linearly related to the [$Ca(OH)_2$] concentration up to its solubility limit of 18 mM [29].

$$\text{Conductivity} = 0.4268\left[Ca(OH)_2\right] \quad (1)$$

where conductivity is in mS/cm and [$Ca(OH)_2$] is in mM, which is also in very good agreement with Burns et al [30]. Since 1 mol of [Ca^{++}] ion was produced from 1 mol of $Ca(OH)_2$ dissolved, the [Ca^{++}] ion concentration could be estimated form the linearity of [$Ca(OH)_2$] concentrations up to its solubility limit. The [OH^-] ion concentration can be calculated from the measured pH values given in Eq. (2) assuming that ionic activity of OH^- ions (a_{OH^-})is relatively equal to [OH^-] ion concentration.

$$\left[OH^-\right] = 10^{(pH-14)} \quad (2)$$

The [Ca^{++}] and [OH^-] ion concentrations estimated from Eq. (1) and Eq. (2) are shown in Fig. 3a. Theoretically, 15 mM [Ca^{++}] and 30 mM [OH^-] ion concentrations would be obtained when a stoichiometric 15 mM of $Ca(OH)_2$ was dissolved in ultrapure water. Moreover, [OH^-] ion concentration would theoretically be two times bigger than the [Ca^{++}] ion concentration. However, as shown in the figure, while the [Ca^{++}] ion concentration was estimated to be about 15 mM, the [OH^-] ion concentration was calculated to be about 25.1 mM, which was smaller than the theoretical value. It was reported that the dissolution of $Ca(OH)_2$ follows the chemical speciation [22]:

$$Ca(OH)_2(s) \rightleftharpoons Ca(OH)_2(aq) \quad pK_a = -2.45 \quad (3)$$

$$Ca(OH)_2(aq) \rightleftharpoons Ca(OH)^+ + OH^- \quad pK_a = -1.37 \quad (4)$$

$$Ca(OH)^+ \rightleftharpoons Ca^{++} + OH^- \quad pK_a = -1.40 \quad (5)$$

Johannsen and Rademacher [31] suggested the following speciation for $Ca(OH)_2$ dissolution, where surface dissociation is important.

$$Ca(OH)_2 \rightarrow Ca^{++} + 2\,OH^-(\text{surface}) \quad (6)$$

$$Ca^{++} + 2\,OH^-(\text{surface}) \rightarrow Ca^{++} + 2\,OH^-(\text{bulk solution}) \quad (7)$$

In the presence of carbonate buffer, additional ions, clusters, and nano-particles could also form [12,13,22].

$$Ca^{++} + HCO_3^- \rightleftharpoons CaHCO_3^+ \quad pK_a = +0.82 \tag{8}$$

$$CaHCO_3^+ \rightleftharpoons CaCO_3(aq) + H^+ \quad pK_a = -7.90 \tag{9}$$

The complex formation of Ca^{++} ions seem to consume some OH^- ions, which cannot diffuse into the pH probe, and therefore, the pH values were measured to be lower than it should be, while the charged species were reported by the conductivity measurement. As can be seen from the figure, the conductivity values started to decrease as soon as the CO_2 bubbles were injected into the solution while the decrease in pH was step-wise. Because the CO_2 injection rate is too slow, the change in pH was relatively slow and it read the same pH value for almost 10 min during crystallization. It seems that the consumption of OH^- ions during and crystallization and CO_2 dissolution initiates other dissociations. Consumption of OH^- ions cause the dissociation of already occurred complexes in the solution such as $Ca(OH)^+$ and $CaHCO_3^+$ ions, which result in releasing the OH^- ions in the solution so that the consumption rate and production rate of OH^- ions were balanced. Therefore, pH stayed almost unchanged for a long period of time during crystallization. It took almost 57 min to consume both Ca^{++} and OH^- concentrations.

Fig. 3b shows the Ca^{++} ion consumption rate calculated from the slope of the conductivity curve. The Ca^{++} ion consumption rate can be related to the $Ca(OH)_2$ consumption rate, $CaCO_3$ crystallization rate, and CO_2 consumption rate according to the overall reaction for $CaCO_3$ crystallization.

$$Ca(OH)_2 + CO_2 \rightarrow CaCO_3 + H_2O \tag{10}$$

As can be seen in the figure, the Ca^{++} ion consumption rate is 6 ± 2 μM/s in 7 l of solution (0.042 ± 0.014 mmole/s) at the earlier stages of crystallization. This rate is also the CO_2 dissolution rate in the $Ca(OH)_2$ solution, which is in good agreement with the literature [32,33]. The decrease in the Ca^{++} concentration also indicate that Ca^{++} ions were consumed in nano crystal formation and attached to the surfaces of the newly produced solid nano-particles used to stabilize the them in the solution. The Ca^{++} consumption rate was relatively slower at the late stage of crystallization due to dissolution-recrystallization mechanism in crystallization [25,26,34,35]. Upon consumption of all Ca^{++} ions, the further dissolution of CO_2 in the solution and the dissolution of the newly synthesized $CaCO_3$ particles started to increase the Ca^{++} ion concentration in the solution so that the Ca^{++} consumption rate became positive for a net Ca^{++} production rate.

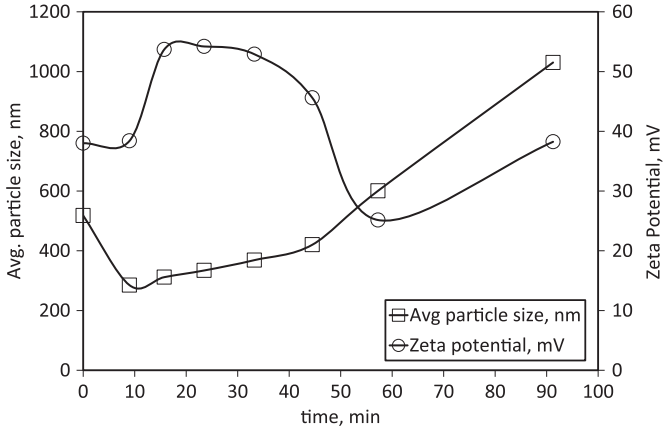

Fig. 4. Change in average particle size and zeta potential values during the progress of $CaCO_3$ crystallization.

The OH^- consumption rate was not shown due to the step change in pH values. However, as can be seen from the overall change of Fig. 3b, the OH^- consumption rate is about double of the Ca^{++} consumption rate.

Fig. 4 shows the zeta potential and average particle size of the particles produced. As shown in the figure, before the crystallization, the average particle size was about 530 nm and the zeta potential was measured to be 40 mV. These particles were mostly $CaCO_3$ particles distributed in the $Ca(OH)_2$ solution as the impurity, which are in good agreement with our previous report [29]. As soon as CO_2 was injected into the solution, the average particle size was measured to be about 250 nm and zeta potential values were increased to 55 mV. As the crystallization progressed, the average particle size was measured to increase to about 400 nm while the zeta potential values was still higher indicating that the newly produced particles were stable in the solution. At the late stage, when Ca^{++} ions were all consumed and pH started to decrease, the zeta potential value started to decrease to about 28 mV and the measured average particle size started to increase. At the end of crystallization, the "measured" average particle size was about 990 nm, which, we believe, is an artifact because, as will be shown in the SEM images below, the increase in number of particles caused the light scattering to a larger size region affecting the DLS measurement for size estimation. The zeta potential value, on the other hand, was 38 mV, which was enough to stabilize the newly synthesized nano-particles. Besides, no any multiple peaks were seen in the size distribution measurements.

Fig. 5 shows the SEM images of the particles obtained at each step of crystallization in the CO_2 bubble reactor. As shown in figure, before the CO_2 injection, at step (0), there was a mixture of large and small particles in solution. These particles were $CaCO_3$ residues remained in the $Ca(OH)_2$ solution as the impurity as indicated in the XRD patterns as shown in Fig. 6. As soon as the CO_2 bubbles were injected in the solution, rice-like $CaCO_3$ particles formed with an average particle size of about 250 nm. Not much aggregation was seen due to the stability effect of $Ca(OH)_2$ solution [29], where the zeta potential values were higher than +30 mV [20]. As the crystallization progress, the particles was shown to grow slightly as their number increased due to newly formed nano-$CaCO_3$ particles. As shown in the images, some of the particles were eroded due to dissolution in the solution. The dissolution rate was significant at step (3) and progressively increased through step (5). These dissolution steps were the reason why the Ca^{++} ion consumption or the crystallization rate was relatively slower compared to the initial step of crystallization as indicated in Fig. 3b. The dissolution of these particles discovered the fact that these particles were indeed in hollow shape with an empty space inside the particles. The growth rate and the dissolution rate were both higher at the edges of the rice-like particles because we think that the edges are the most energetic parts [36]. Interestingly, the hollow openings to the edges were closed up at the end of crystallization at step (6) and step (7) as a result of the dissolution and recrystallization of $CaCO_3$ particles in the solution [25,26,34,35].

The diffraction peaks in XRD was shown in Fig. 6. The 2θ value at 29.468o, and the sharp peaks at the d-spacing 3.02864, 1.9166 and 1.8796 represent the well characterized (104) calcite form of $CaCO_3$. There was no any different peak detected showing any impurity or any different $CaCO_3$ crystalline form.

Fig. 7 shows a possible mechanism for the formation of the rice-like hollow nano-$CaCO_3$ particles. Once the CO_2 bubble was introduced into the $Ca(OH)_2$ solution, it will dissolve and its concentration increases around the bubbles, which reacts with the available Ca^{++} ions in the solution. The newly produced $CaCO_3$ particles would be $CaCO_3$ crystallite particles [7,10,37] of about 40 nm as we calculated from the (104) peak of the XRD pattern of

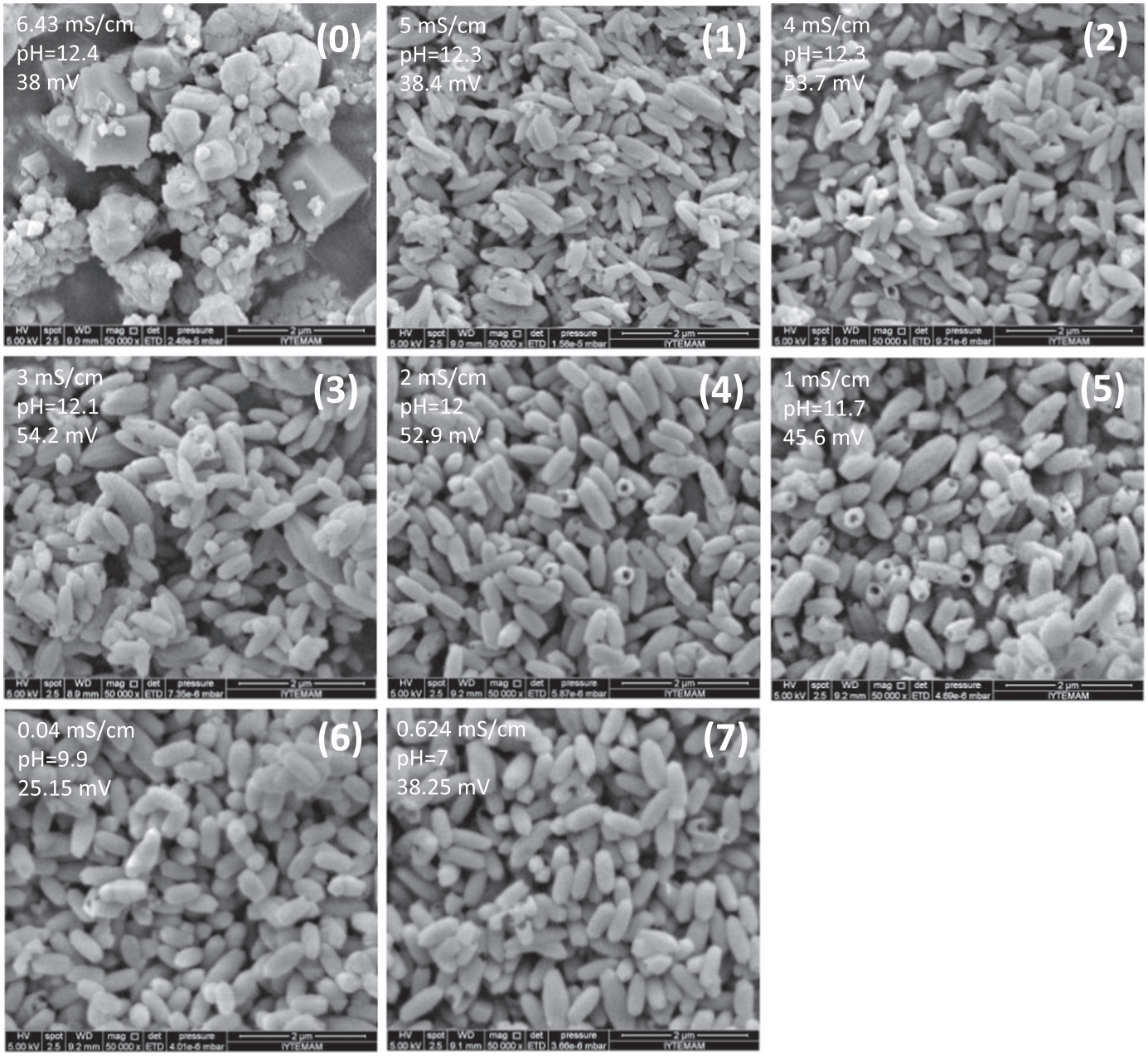

Fig. 5. SEM images showing the progress in the rice-like hollow nano-$CaCO_3$ formation.

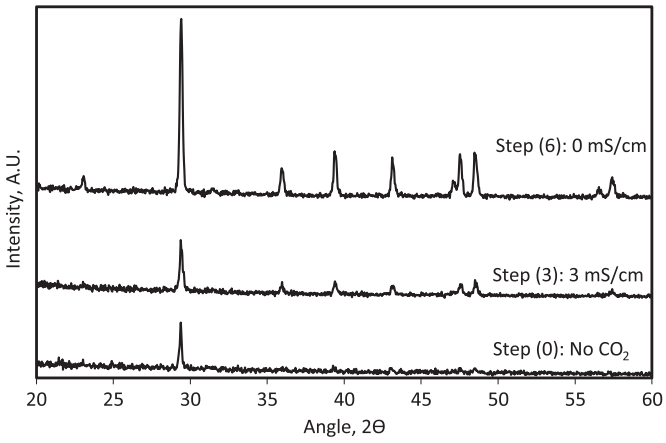

Fig. 6. XRD patterns of the rice-like hollow nano-$CaCO_3$ particles.

the $CaCO_3$ particles using the Sheerer Equation [38]. As shown in Fig. 7a, these nano crystallites aggregate with the available Ca^{++} and CO_3^{2-} and other charged clusters such as $CaHCO_3^{+}$ and $Ca(OH)^{+}$ to form rice-like $CaCO_3$ particles growing at the edges. Arrows show the progress or dissolution in the crystallization. As shown in Fig. 7b, the crystallites on these newly developed nano-particles are not stable and vulnerable to dissolve. As crystallization progress, these particles can disintegrate and dissolve in the solution starting from the edges, and at the surfaces when they come across the close territory of the CO_2 bubbles, where pH is lower and there is an imbalance between the ions. As shown in Fig. 7c and d, the progress in dissolution at the edges result in hollow nano-$CaCO_3$ particles. When all the Ca^{++} ions were consumed in the solution, pH starts to decrease, which facilitates the dissolution, increasing further the Ca^{++} concentration in the solution. This process causes the recrystallization of the particles leading to close up the edges of the hollow $CaCO_3$ particles with an empty

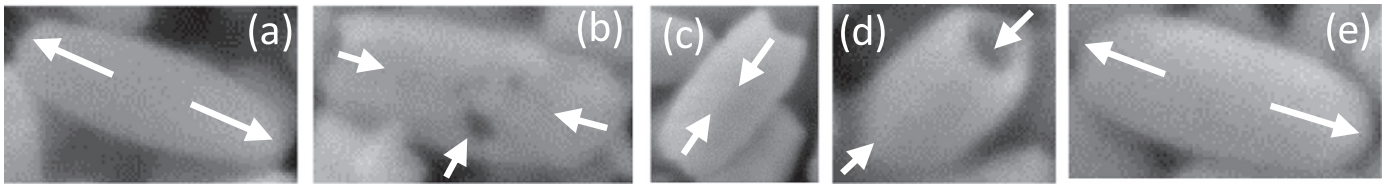

Fig. 7. Possible mechanism for the formation of the rice-like hollow nano-$CaCO_3$ synthesis. Arrows show the progress or dissolution in the crystallization.

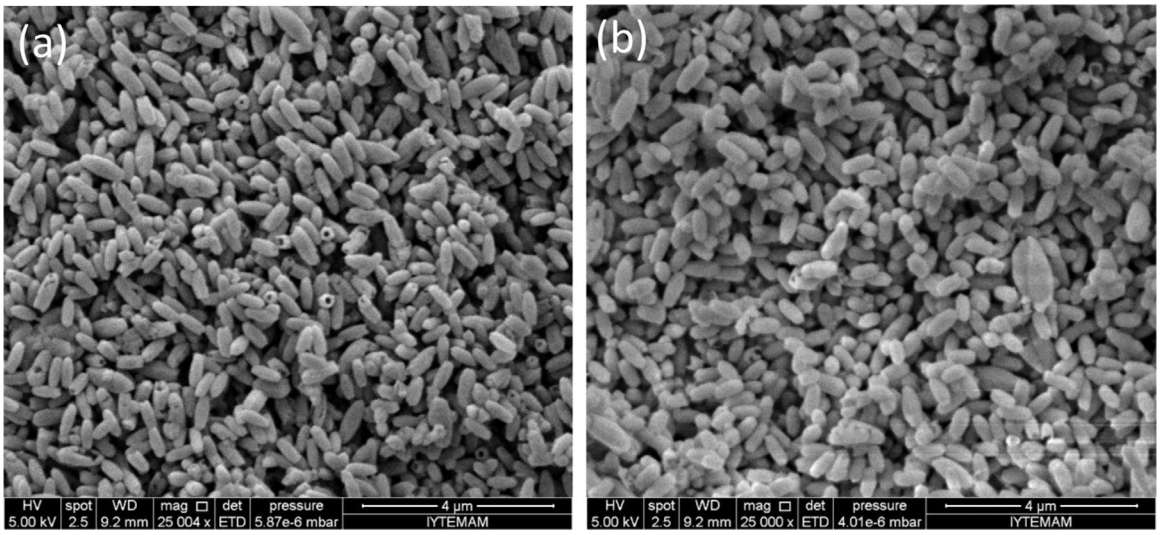

Fig. 8. SEM images of rice-like hollow nano-$CaCO_3$ particles, (a) with open pores, and (b) with closed pores, with a monodisperse particle size distribution.

space inside.

It is important to understand the chemistry behind formation and close-up of the hollow structures in nano-$CaCO_3$ synthesis. We have reported in our previous paper that the solubility values for $Ca(OH)_2$ and $CaCO_3$ are about 20 mM and 0.1 mM, respectively [29]. Therefore, the solution was initially undersaturated with respect to $Ca(OH)_2$ and supersaturated with respect to $CaCO_3$. However, the supersaturation conditions can change through the progress of the crystallization leading to the dissolution of the newly synthesized $CaCO_3$ particles and/or close-up of pores as a result of recrystallization. Because this is our first report on the formation of pores in $CaCO_3$ synthesis, there are a lot to do to understand the chemistry behind the formation of such structures with a well-defined chemical models, such as PHREEQC [39], and others [40].

As can be seen in the SEM images of the rice-like hollow nano-$CaCO_3$ particles in Fig. 8, these particles have a monodisperse particle size distribution without aggregation. These hollow nanoparticles have numerous advantages. For instance, the bulk density of these particles were measured by packing them in a measure and estimated their weight per volume. Their bulk density was about 0.95 g/cm^3 compared to 2.74 g/cm^3 of the density of crystal calcite. The BET surface area of the open-pore and close-pore calcite was measured to be about 15 m^2/g and 12 m^2/g, respectively. Due to weight reduction and high surface area, the hollow rice-like nano calcite particles could be used in composite materials, plastics, cement, paint, paper manufacturing, etc. [41–46]. Most importantly, as we were searching for a candidate for the inorganic material for drug loading, drugs can be trapped within these hollow nano-$CaCO_3$ particles to effectively and efficiently deliver them to the tumors and cancer cells with some modifications [19,47–51]. In the future, methods will be developed to synthesize featured hollow nano-$CaCO_3$ particles for drug loading and cancer therapy.

4. Conclusions

Rice-like hollow nano-$CaCO_3$ particles were produced by slow addition of CO_2 bubbles into the $Ca(OH)_2$ solution. The estimated OH^- ion concentration was lower than its theoretical value due to complex formation in the presence of Ca^{++} ions, for which pH reading was lower than expected while conductivity reading was satisfactory to estimate the charged species. The Ca^{++} ion consumption rate was relatively higher at the early stage of crystallization, however, it was slower at the late stage of crystallization due to dissolution-recrystallization of the newly synthesized $CaCO_3$ particles. Dissolution was faster at the edges of the rice-like particles. At the late stages, when Ca^{++} ions were consumed and pH decreased, recrystallization resulted in close-up of the edges of the particles leading to the formation of fine hollow nano-$CaCO_3$ particles. XRD patterns of the particles indicated that the particles were all the calcite form of $CaCO_3$. These particles were thought to be used in drug loading and cancer treatment applications with some modifications.

Acknowledgments

The Scientific and Technological Research Council of Turkey (TUBITAK) is highly appreciated for the research grant with the project number 110M104.

References

[1] Y. Lin, H.B. Chen, C.M. Chan, J.S. Wu, High impact toughness polypropylene/$CaCO_3$ nanocomposites and the toughening mechanism, Macromolecules 41 (2008) 9204–9213.

[2] S.Se Sant'Anna, D.Ad Souza, D.Md Araujo, Cd.F. Carvalho, M.I. Yoshida, Physico-chemical analysis of flexible polyurethane foams containing commercial calcium carbonate, Mater. Res. 11 (2008) 433–438.

[3] J.G. Carmona, J.G. Morales, R. Rodriguez-Clemente, Rhombohedral-scalenohedral calcite transition produced by adjusting the solution electrical conductivity in the system Ca(OH)(2)–CO_2–H_2O, J. Colloid Interface Sci. 261 (2003) 434–440.
[4] J.G. Carmona, J.G. Morales, J.F. Sainz, E. Loste, R.R. Clemente, The mechanism of precipitation of chain-like calcite, J. Cryst. Growth 262 (2004) 479–489.
[5] J.F. Chen, Y.H. Wang, F. Guo, X.M. Wang, C. Zheng, Synthesis of nanoparticles with novel technology: high-gravity reactive precipitation, Ind. Eng. Chem. Res. 39 (2000) 948–954.
[6] M. Ukrainczyk, J. Kontrec, V. Babic-Ivancic, L. Brecevic, D. Kralj, Experimental design approach to calcium carbonate precipitation in a semicontinuous process, Powder Technol. 171 (2007) 192–199.
[7] D. Gebauer, A. Volkel, H. Colfen, Stable prenucleation calcium carbonate clusters, Science 322 (2008) 1819–1822.
[8] M. Kellermeier, D. Gebauer, E. Melero-Garcia, M. Drechsler, Y. Talmon, L. Kienle, H. Colfen, J.M. Garcia-Ruiz, W. Kunz, Colloidal stabilization of calcium carbonate prenucleation clusters with silica, Adv. Funct. Mater. 22 (2012) 4301–4311.
[9] S. Kilic, E. Ozdemir, Toward synthesis of $CaCO_3$, J. Cryst. Growth (2015) (submitted for publication).
[10] E.M. Pouget, P.H.H. Bomans, J.A.C.M. Goos, P.M. Frederik, G. de With, N.A.J. M. Sommerdijk, The initial stages of template-controlled $CaCO_3$ formation revealed by cryo-TEM, Science 323 (2009) 1455–1458.
[11] R. Agnihotri, S.K. Mahuli, S.S. Chauk, L.S. Fan, Influence of surface modifiers on the structure of precipitated calcium carbonate, Ind. Eng. Chem. Res. 38 (1999) 2283–2291.
[12] L. Holysz, E. Chibowski, A. Szczes, Influence of impurity ions and magnetic field on the properties of freshly precipitated calcium carbonate, Water Res. 37 (2003) 3351–3360.
[13] P. Moulin, H. Roques, Zeta potential measurement of calcium carbonate, J. Colloid Interface Sci. 261 (2003) 115–126.
[14] S. Pourchet, I. Pochard, F. Brunel, D. Perrey, Chemistry of the calcite/water interface: influence of sulfate ions and consequences in terms of cohesion forces, Cem. Concr. Res. 52 (2013) 22–30.
[15] A.W. Xu, Y.R. Ma, H. Colfen, Biomimetic mineralization, J. Mater. Chem. 17 (2007) 415–449.
[16] Q. Liu, Q. Wang, L. Xiang, Influence of poly acrylic acid on the dispersion of calcite nano-particles, Appl. Surf. Sci. 254 (2008) 7104–7108.
[17] K.S. Seo, C. Han, J.H. Wee, J.K. Park, J.W. Ahn, Synthesis of calcium carbonate in a pure ethanol and aqueous ethanol solution as the solvent, J. Cryst. Growth 276 (2005) 680–687.
[18] Y. Sheng, B. Zhou, J.Z. Zhao, N. Tao, K.F. Yu, Y.M. Tian, Z.C. Wang, Influence of octadecyl dihydrogen phosphate on the formation of active super-fine calcium carbonate, J. Colloid Interface Sci. 272 (2004) 326–329.
[19] Y. Boyjoo, V.K. Pareek, J. Liu, Synthesis of micro and nano-sized calcium carbonate particles and their applications, J. Mater. Chem. A 2 (2014) 14270–14288.
[20] M. Kes, Determination of the particle interactions - rheology- surface roughness relationshipmfor dental ceramics in: Department of Chemistry, Izmir Institute of Technology, Izmir, 2007, pp. 111.
[21] M. Kosmulski, pH-dependent surface charging and points of zero charge. IV update new approach, J. Colloid Interface Sci. 337 (2009) 439–448.
[22] E. Chibowski, L. Hotysz, A. Szczes, Time dependent changes in zeta potential of freshly precipitated calcium carbonate, Colloid Surf. A 222 (2003) 41–54.
[23] J.G. Carmona, J.G. Morales, J.F. Sainz, R.R. Clemente, Morphological characteristics and aggregation of calcite crystals obtained by bubbling CO_2 through a $Ca(OH)_2$ suspension in the presence of additives, Powder Technol. 130 (2003) 307–315.
[24] M. Kitamura, H. Konno, A. Yasui, H. Masuoka, Controlling factors and mechanism of reactive crystallization of calcium carbonate polymorphs from calcium hydroxide suspensions, J. Cryst. Growth 236 (2002) 323–332.
[25] J.D. Rodriguez-Blanco, S. Shaw, L.G. Benning, The kinetics and mechanisms of amorphous calcium carbonate (ACC) crystallization to calcite, via vaterite, Nanoscale 3 (2011) 265–271.
[26] C.Y. Tai, F.B. Chen, Polymorphism of $CaCO_3$ precipitated in a constant-composition environment, Aiche J. 44 (1998) 1790–1798.
[27] G.W. Yan, J.H. Huang, J.F. Zhang, C.J. Qian, Aggregation of hollow $CaCO_3$ spheres by calcite nanoflakes, Mater. Res. Bull. 43 (2008) 2069–2077.
[28] P.Q. Yuan, Z.M. Cheng, Z.M. Zhou, W.K. Yuan, R. Semiat, Zeta potential on the anti-scalant modified sub-micro calcite surface, Colloid Surf. A 328 (2008) 60–66.
[29] S. Kilic, G. Toprak, E. Ozdemir, Stability of $CaCO_3$ in Ca(OH)(2) solution, Int. J. Miner. Process. 147 (2016) 1–9.
[30] J.R. Burns, J.J. Jachuck, Monitoring of $CaCO_3$ production on a spinning disc reactor using conductivity measurements, Aiche J. 51 (2005) 1497–1507.
[31] K. Johannsen, S. Rademacher, Modelling the kinetics of calcium hydroxide dissolution in water, Acta Hydrochim. Hydrobiol. 27 (1999) 72–78.
[32] R.Y. Lin, J.Y. Zhang, Y.Q. Bai, Mass transfer of reactive crystallization in synthesizing calcite nanocrystal, Chem. Eng. Sci. 61 (2006) 7019–7028.
[33] F. Takemura, Y. Matsumoto, Dissolution rate of spherical carbon dioxide bubbles in strong alkaline solutions, Chem. Eng. Sci. 55 (2000) 3907–3917.
[34] J. Rieger, M. Kellermeier, L. Nicoleau, Formation of nanoparticles and nanostructures-an industrial perspective on $CaCO_3$, Cem. Polym. Angew. Chem. Int. Ed. 53 (2014) 12380–12396.
[35] J.D. Rodriguez-Blanco, S. Shaw, P. Bots, T. Roncal-Herrero, L.G. Benning, The role of pH and Mg on the stability and crystallization of amorphous calcium carbonate, J. Alloy. Compd. 536 (2012) S477–S479.
[36] M. Xu, X.M. Hu, K.G. Knauss, S.R. Higgins, Dissolution kinetics of calcite at 50–70 °C: an atomic force microscopic study under near-equilibrium conditions, Geochim. Cosmochim. Acta 74 (2010) 4285–4297.
[37] J. Rieger, J. Thieme, C. Schmidt, Study of precipitation reactions by X-ray microscopy: $CaCO_3$ precipitation and the effect of polycarboxylates, Langmuir 16 (2000) 8300–8305.
[38] M. Schmidt, T. Stumpf, C. Walther, H. Geckeis, T. Fanghanel, Phase transformation in $CaCO_3$ polymorphs: a spectroscopic, microscopic and diffraction study, J. Colloid Interface Sci. 351 (2010) 50–56.
[39] P. Huber, Kinetics of CO_2 Stripping and its effect on the saturation state of $CaCO_3$ upon aeration of a $CaCO_3$–CO_2–H_2O system: application to scaling in the papermaking process, Ind. Eng. Chem. Res. 50 (2011) 13655–13661.
[40] Z. Duan, D. Li, Coupled phase and aqueous species equilibrium of the H_2O–CO_2–NaCl–$CaCO_3$ system from 0 to 250 °C, 1 to 1000 bar with NaCl concentrations up to saturation of halite, Geochim. Cosmochim. Acta 72 (2008) 5128–5145.
[41] B. Beskova, M. Starkova, E. Sarka, J. Gojny, Z. Bubnik, Application of carbonatation lime as a filler for adhesives, Zuckerindustrie 134 (2009) 486–490.
[42] J.S.D. Campos, A.A. Ribeiro, C.X. Cardoso, Preparation and characterization of PVDF/$CaCO_3$ Composites, Mater. Sci. Eng. B-Solid 136 (2007) 123–128.
[43] T.D. Lam, T.V. Hoang, D.T. Quang, J.S. Kim, Effect of nanosized and surface-modified precipitated calcium carbonate on properties of $CaCO_3$/polypropylene nanocomposites, Mater. Sci. Eng. A-Struct. 501 (2009) 87–93.
[44] Y. Sheng, J.Z. Zhao, B. Zhou, X.F. Ding, Y.H. Deng, Z.C. Wang, In situ preparation of $CaCO_3$/polystyrene composite nanoparticles, Mater. Lett. 60 (2006) 3248–3250.
[45] L. Sorrentino, F. Berardini, M.R. Capozzoli, S. Amitrano, S. Iannace, Nano/micro ternary composites based on PP, nanoclay, and $CaCO_3$, J. Appl. Polym. Sci. 113 (2009) 3360–3367.
[46] Y. Wen, L. Xiang, Y. Jin, Synthesis of plate-like calcium carbonate via carbonation route, Mater. Lett. 57 (2003) 2565–2571.
[47] T. Ikoma, T. Tonegawa, H. Watanaba, G.P. Chen, J. Tanaka, Y. Mizushima, Drug-supported microparticles of calcium carbonate nanocrystals and its covering with hydroxyapatite, J. Nanosci. Nanotechnol. 7 (2007) 822–827.
[48] D. Preisig, D. Haid, F.J.O. Varum, R. Bravo, R. Alles, J. Huwyler, M. Puchkov, Drug loading into porous calcium carbonate microparticles by solvent evaporation, Eur. J. Pharm. Biopharm. 87 (2014) 548–558.
[49] N. Qiu, H.B. Yin, B.Z. Ji, N. Klauke, A. Glidle, Y.K. Zhang, H. Song, L.L. Cai, L. Ma, G.C. Wang, L.J. Chen, W.W. Wang, Calcium carbonate microspheres as carriers for the anticancer drug camptothecin, Mater. Sci. Eng. C-Mater. 32 (2012) 2634–2640.
[50] A.A. Weiner, D.M. Shuck, J.R. Bush, V.P. Shastri, In vitro degradation characteristics of photocrosslinked anhydride systems for bone augmentation applications, Biomaterials 28 (2007) 5259–5270.
[51] Y. Zhao, Z. Luo, M.H. Li, Q.Y. Qu, X. Ma, S.H. Yu, Y.L. Zhao, A preloaded amorphous calcium carbonate/doxorubicin@silica nanoreactor for pH-responsive delivery of an anticancer drug, Angew. Chem. Int. Ed. 54 (2015) 919–922.